Crossed Molecular Beam Study of the Reaction Cl + O_3

Jingsong Zhang*,† and Yuan T. Lee

Chemical Sciences Division, Lawrence Berkeley National Laboratory, and Department of Chemistry, University of California, Berkeley, California 94720

Received: March 6, 1997; In Final Form: May 29, 1997[⊗]

The reaction of ground-state (^2P_J) chlorine atom with ozone molecule was studied by the crossed molecular beams technique at four different center-of-mass (CM) collision energies ranging from 6 to 32 kcal/mol. CM translational energy and angular distributions of the products were derived from experimental measurements. A significant fraction of the total available energy is channeled into the products' translation, and the ClO product is sideways and forward scattered with respect to the Cl atom. Product translational energy release depends on the CM scattering angle, with higher values at small CM angles. With the increase of collision energy, product translational energy increases, and the ClO product is scattered to a more forward direction. The reaction Cl + O_3 proceeds through a direct reaction mechanism. The Cl atom is most likely to attack the terminal oxygen atom of the ozone molecule.

I. Introduction

The reaction Cl + O_3 → ClO + O_2 is of fundamental importance in stratospheric chemistry.[1] It plays a key role in catalytic ozone destruction cycles. Currently, it is believed that the following two catalytic cycles are responsible for most of the Antarctic stratosphere ozone loss:[2−6]

(I) ClO dimer mechanism:[2]

$$2(Cl + O_3 \rightarrow ClO + O_2)$$

$$2ClO + M \rightarrow (ClO)_2$$

$$(ClO)_2 + h\nu \rightarrow Cl + ClOO$$

$$ClOO + M \rightarrow Cl + O_2 + M$$

$$\text{net:} \quad 2O_3 \rightarrow 3O_2$$

(II) ClO/BrO mechanism:[3]

$$Cl + O_3 \rightarrow ClO + O_2$$

$$Br + O_3 \rightarrow BrO + O_2$$

$$ClO + BrO \rightarrow Cl + Br + O_2$$

$$\text{net:} \quad 2O_3 \rightarrow 3O_2$$

Present calculations indicate that the ClO dimer mechanism (I) accounts for 75% and the ClO/BrO mechanism (II) accounts for 20% of the Antarctic stratosphere ozone loss.[3−6]

A large number of kinetic studies on the Cl + O_3 and similar reactions such as the Br + O_3 reaction have been carried out.[7−12] Measurements made in these studies of reaction rate coefficients and their temperature dependences provide a valuable data base for stratospheric chemistry modeling. It has been found that for X + O_3 (X = O(^{3}P), F, Cl, and Br) reactions, with the exception of the H + O_3 reaction, the preexponential factors were all very close to 2.2×10^{-11} cm^3 molecule^{-1} s^{-1} and were insensitive to the reaction exothermicity.[11,12] The rate coefficients for the reactions X + O_3 were found to correlate with electron affinities of the radical atoms instead of with the reaction exothermicity.[9] For reactions of O_3 with diatomic radicals such as NO, OH, and SO, there was similarly little variation in the preexponential factors; rather, all such values were close to 2.2×10^{-12} cm^3 molecule^{-1} s^{-1}.[11,12] Largely on the basis of these findings, it was suggested that the transition-state structures of these reactions were insensitive to the reactant X, and the X + O_3 reactions proceeded via early transition states that best resembled the reactant ozone.[9,10] Because of the correlation of the radical electron affinities with the reaction rate constants, it was also suggested that in X + O_3 reactions electron density might have been transferred from the highest occupied ozone molecular orbital to the singly occupied radical molecular orbital.[9,10]

Asymmetric ClO_3 (ClO•OO) has been postulated as a possible reaction intermediate.[13] However, Carter and Andrews' matrix isolation study of the Cl + O_3 reaction showed no observable infrared absorptions of a possible asymmetric ClO_3 radical species, suggesting that the asymmetric ClO_3 was not a stable species even in the low-temperature matrix.[14] Meanwhile, the ClO radical produced from this matrix reaction was clearly identified in the infrared absorption spectra. It may be surmised that if the asymmetric ClO_3 were the possible reaction intermediate of the Cl + O_3 reaction, this reaction probably would not proceed through a long-lived complex.

McGrath and Norrish carried out a pioneer flash photolysis study on the Cl_2−O_3 reaction system.[15] Immediately after the flash photolysis of Cl_2, in the time range of several microseconds, a strong $v'' = 0$ progression of ClO was observed in the absorption spectra, with the maximum value of v'' possibly being as high as 5. Some vibrational relaxation of the nascent ClO product had occurred on the time scale of the flash photolysis study; however, it was quite evident that the ClO product from the Cl + O_3 reaction had considerable vibrational excitation. Recently, Baumgärtel and Gericke detected the ClO product from the Cl + O_3 reaction by using two-photon fluorescence excitation, and they suggested an inverted nascent ClO vibrational distribution.[16] Quantitative analysis of this distribution was given by Matsumi and co-workers;[17] by using vacuum-ultraviolet laser-induced fluorescence, they measured a strongly inverted nascent ClO vibrational distribution (up to $v = 5$) from the Cl + O_3 reaction at room temperature. They also suggested

† Present address: Department of Chemistry, University of California, Riverside, CA 92521-0403. Fax 909-787-4713; E-mail jszhang@ucrac1.ucr.edu.

⊗ Abstract published in *Advance ACS Abstracts,* August 1, 1997.

S1089-5639(97)00859-1 CCC: $14.00 © 1997 American Chemical Society

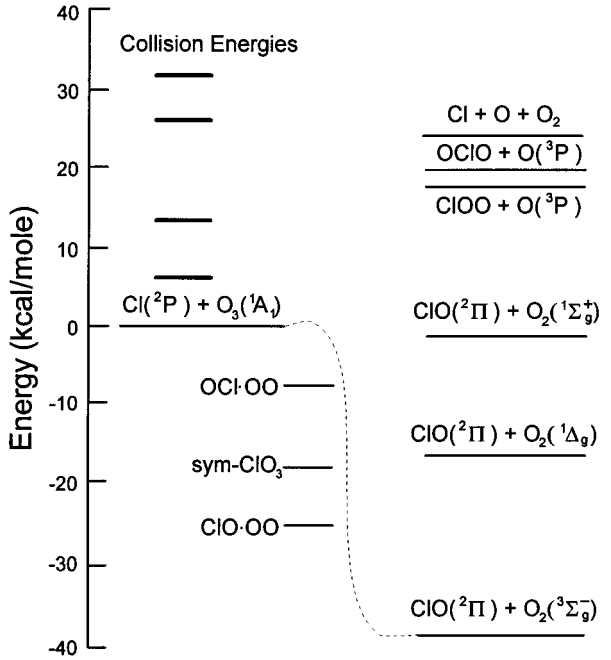

Figure 1. Energy level diagram of the Cl + O_3 system. Thermodynamic data are derived from refs 12b and 21 (for three chlorine trioxides). The solid lines stand for the collision energies in the experiment.

that the nascent distribution peaked at $v = 8 \pm 2$ by extrapolating a linear surprisal plot of the vibration populations.[17]

Electronically excited oxygen molecule products $O_2(^1\Delta_g)$ and $O_2(^1\Sigma_g^+)$ are energetically possible (Figure 1); however, they have not been observed in bulk thermal experiments. Vanderzanden and Birks tried to find the electronically excited product $O_2(^1\Sigma_g^+)$ of the Cl + O_3 reaction in a flow tube experiment by detecting O atoms produced from a secondary reaction between the product $O_2(^1\Sigma_g^+)$ and O_3.[18] Under the assumption that all the oxygen atoms detected in their system originated from the secondary reaction $O_2(^1\Sigma_g^+) + O_3 \rightarrow 2O_2(^3\Sigma_g^-) + O$, they estimated the branching ratio of the $O_2(^1\Sigma_g^+)$ channel to be $(1-5) \times 10^{-3}$. In a similar effort, Choo and Leu studied the possible formation of $O_2(^1\Delta_g)$ and $O_2(^1\Sigma_g^+)$ by using the flow-discharge/chemiluminescence detection method.[19] They also failed to detect any $O_2(^1\Delta_g)$ and $O_2(^1\Sigma_g^+)$ chemiluminescence signals and set the upper limits of the branching ratios for $O_2(^1\Sigma_g^+)$ and $O_2(^1\Delta_g)$ channels as $\leq 5 \times 10^{-4}$ and $\leq 2.5 \times 10^{-2}$, respectively. Both studies showed that production of the electronically excited oxygen molecules $O_2(^1\Delta_g)$ and $O_2(^1\Sigma_g^+)$ in the Cl + O_3 reaction was negligible.

There have been few theoretical studies of the Cl + O_3 reaction. Farantos and Murrell used the many-body expansion method to derive an analytic function for the potential energy surface (PES) of the ground-state $ClO_3(^2A)$.[20] In this functional form, relative to the energies of the separated atoms, ClO_3 PES was taken as a sum of the interaction energies of the atoms in pairs [V^i(ClO) and V^i(OO)], of the atoms in threes [$V^i(ClO_2)$ and $V^i(O_3)$], and a four-body term [$V(ClO_3)$]. Including all the two-, three-, and four-body terms, they located an early transition state for the collinear collision pathway in which Cl attacked along the axis of one O−O bond. The reaction barrier height along this collinear pathway was 0.34 kcal/mol, an estimation that appeared to be consistent with the experimental measurement of a 0.5 kcal/mol activation energy.[10] Classic trajectory calculations were carried out on this PES at four collision energies corresponding to Maxwell mean velocities that ranged from 200 to 600 K with the O_3 molecule in its vibrational ground state. The rate constant at room temperature was estimated by using the cross sections generated from the trajectory calculations; its value, 1.34×10^{-11} cm^3 molecule^{-1} s^{-1}, was consistent with the experimental value of 1.2×10^{-11} cm^3 molecule^{-1} s^{-1}. The trajectory calculations also provided some insight into the dynamics of this reaction. It was calculated that at 300 K the ClO product was predominantly forward scattered with respect to the Cl atom in the CM system. Lack of a forward−backward symmetry showed no long-lived complex formation along this collinear pathway. The calculations indicated that at 300 K about 49% of the total available energy went into translation of the products while 20% and 19% went into ClO vibrational and rotational energy, respectively, and only 4% and 9% went into O_2 vibrational and rotational energy. They also predicted that $v = 1$ was the most probable vibrational state of ClO, but vibrational states up to $v = 8$ would be populated while almost all the O_2 would be in the ground vibrational state. The substantial amount of ClO vibrational energy shown in the calculations was due to the early transition state located in the entrance valley. The O−O bond length, however, did not change much during the reaction, and consequently there was much less O_2 vibrational excitation.

Rathmann and Schindler carried out *ab initio* calculations on geometries and thermodynamic properties of three chlorine trioxide isomers: ClO·O_2 ($\Delta H_{f,0K}$ = 41 kcal/mol), OCl·O_2 ($\Delta H_{f,0K}$ = 58 kcal/mol), and *sym*-ClO_3 ($\Delta H_{f,0K}$ = 48 kcal/mol).[21] It was shown that the formation of the asymmetric ClO·O_2 adduct by association of O_2 and ClO was endothermic by 13 kcal/mol; i.e., the relative energy of the asymmetric ClO·O_2 intermediate lies above that of the separated products ClO and O_2 (Figure 1). Recently, Radom and co-workers investigated the ClO_3 isomers in greater detail with higher level *ab initio* calculations.[22] As in Rathmann and Schindler's study, on the UMP2/6-31G(d) PES, a stable ClOOO isomer was found with a similar relative energy. Furthermore, higher level *ab initio* calculations showed that the ClOOO structure was not stable on the RMP2/6-31G(d) and the QCISD(T)/6-31G(d) surfaces.[22] Radom and co-workers concluded that their higher level *ab initio* calculations suggested the absence of a stable covalently bound (as opposed to van der Waals) ClOOO complex. Both *ab initio* investigations on the ClO_3 isomers[21,22] indicate that the Cl + O_3 reaction should not proceed through a long-lived complex if this asymmetric ClO_3 is the reaction intermediate.

Schaefer and co-workers have used *ab initio* quantum mechanical methods to determine the key features of the H + O_3 PES.[23] The authors expected the key features of the H + O_3 PES to be transferable to X + O_3 (X = Cl, OH, NO, and NH_2) systems because the electronic structure of ozone played a dominant role in determining these key features. However, they could not locate a planar transition state for a direct O atom abstraction; instead, they suggested that the H + O_3 reaction proceeded through a nonplanar pathway in which the H atom attacked vertically to the ozone molecule plane. Most of the reaction exothermicity was released while the H−O bond was being formed, channeling energy specifically into OH vibration, in accord with experimental results from the chemiluminescence work by Polanyi and co-workers.[24] However, the experiment also showed a large ratio of OH vibrational energy (90% of the total energy) to OH rotational energy (∼3% of the total energy), which led Polanyi and co-workers to suggest that the PES favored a collinear HOO approach and the H + O_3 reaction was restricted to a narrow range of impact parameters.[24] There is certainly a discrepancy between the *ab initio* calculation and the conclusion derived from the experimental results on the H + O_3 reaction. Furthermore, if indeed the key features of the H + O_3 PES were transferable to the Cl + O_3 system, they would be quite different from those found in the semiem-

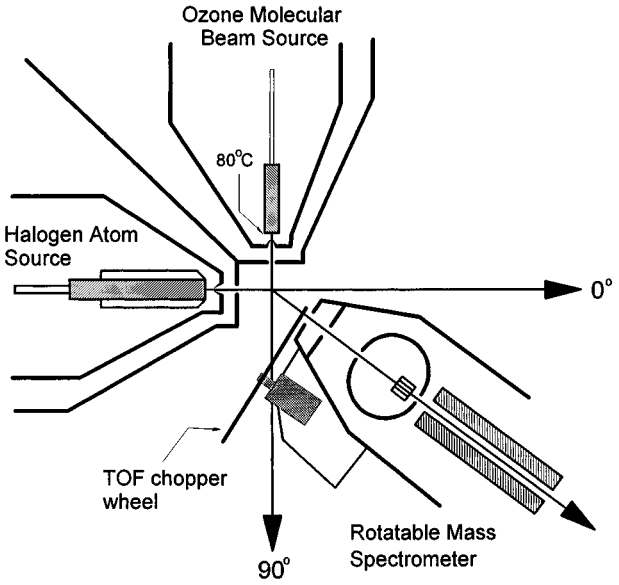

Figure 2. Schematic of the crossed molecular beam apparatus. The direction of Cl beam (Cl velocity vector) is defined as laboratory angle $\Theta = 0°$, and the direction of ozone velocity vector is $\Theta = 90°$.

pirical calculations.[20] An *ab initio* calculation of the Cl + O_3 system itself would be very helpful.

The Cl + O_3 reaction mechanism is not yet very clear. The goal of the present work is to probe Cl + O_3 reaction dynamics under well-defined single-collision conditions. We have carried out a crossed molecular beam study for this reaction at four collision energies. CM angular and translational energy distributions are derived from experimental measurements. Using the obtained information, we hope to provide more insight into the detailed dynamics of this important reaction.

II. Experimental Section

The universal crossed molecular beam apparatus used in this study has been previously described in detail.[25] The beams and detector arrangement is shown in Figure 2. Continuous supersonic chlorine atom and ozone molecular beams were two-stage differentially pumped and were crossed at 90° in the main collision chamber held at a vacuum of $\sim 10^{-7}$ Torr. The scattered products were detected by a triply differentially pumped mass spectrometric detector which rotated in the plane of the two beams with respect to the crossing point. The mass spectrometric detector is composed of a Brink-type electron impact ionizer,[26] an Extrel quadrupole mass spectrometer, and a scintillation-based Daly ion detector.[27] The typical electron energy and ion energy were 180 and 90 eV, respectively. The size of the collision zone was $3 \times 3 \times 3$ mm^3, and under normal conditions the whole collision zone was viewed by the detector.

Chlorine atom beam was produced by thermal dissociation of Cl_2 in rare gas mixtures in a resistively heated high-density graphite nozzle source.[28] Mixtures of 10% Cl_2 in argon, 10% Cl_2 in 8% argon and 82% helium, 5% Cl_2 in helium, and 1% Cl_2 in helium were used. The total stagnation pressure of the beam was typically 700 Torr. The high-temperature graphite source had a nozzle of 0.12 mm diameter and was heated to ~1400−1600 °C. The nozzle temperature was constantly monitored by type C (tungsten−5% rhenium vs tungsten−26% rhenium) thermocouples on the graphite heater and was frequently checked by an optical pyrometer and by beam velocities of pure rare gases from time-of-flight (TOF) measurements. After correction for graphite emissivity and view-port Plexiglas absorption, the optical pyrometric measurements agreed reasonably well with the rare-gas TOF temperature measurements. A conical graphite skimmer with a 1.0 mm diameter orifice was positioned 7.6 mm downstream from the nozzle. A set of collimating slits further downstream on the differential wall defined the beam to 3° in full width. A large fraction of Cl_2 was thermally dissociated, as observed by mass spectrometric measurements of [Cl]/[Cl_2] ratio in the beam. Heating power for the high-temperature graphite source was carefully maintained constant throughout the experiment to ensure a stable Cl atom beam. Perfluoropolyether (PFPE) pumping fluids (Fomblin 25/6 for mechanical pump and Fomblin 25/9 for diffusion pump) were used for the pumping system.

Ozone used in this experiment was generated by a commercial ozonator (OREC, 03v1-0). The ozonator output (10% ozone, 90% oxygen) was passed through a Pyrex glass trap filled with coarse silica gel cooled to −78 °C in a dry ice/acetone slush.[29−31] After 1−3 h of running time, a sufficient amount of deep blue ozone along with a small amount of oxygen was adsorbed on the silica gel. The trap was then transferred to a temperature-controlled cooling bath (FTS Multicool System, MC-4-60A-1), and a gas mixture was generated by passing rare gas to carry the desorbing ozone out of the trap. Ozone concentration was continuously monitored by ultraviolet absorption of the gas mixture in a 1×1 cm^2 quartz flow cell at wavelength of 280 nm prior to its entry into the ozone molecular beam source. After running the ozone beam for 1−2 h, the small amount of O_2 in the silica gel trap was well purged by the inert carrier gas, and the system was also well passivated. The stabilized ozone gas mixture was typically maintained at a concentration of 7% with 300 Torr of total pressure, giving a reasonable transmission at 280 nm.[12,32,33] Because the ozone in the silica gel trap was gradually depleted, operation temperature of the cooling bath was adjusted in the range −60 to −30 °C to maintain a constant ozone concentration. The ozone beam source had a nozzle of 0.12 mm in diameter. To minimize the formation of ozone dimers, the nozzle tip was heated to ~80 °C. The ozone beam was skimmed by a stainless steel skimmer with a 0.5 mm diameter orifice placed at a nozzle−skimmer distance of 7.6 mm. The beam was further defined by the collimating slits on the differential wall to have a full width of 3° before it entered the main chamber. The [O_3]/[O_2] ratio was typically ~3 determined from the mass spectrometric measurement. Since the Cl + O_2 reaction was energetically impossible in this experiment, the presence of small amount of O_2 in the beam was not a problem.

The TOF technique was used to measure velocity distributions of the Cl and O_3 beams. A stainless steel wheel 17.8 cm in diameter with four 0.78 mm slots equally spaced around its circumference was installed in front of the detector. The wheel was spun at 300 Hz, and the modulated beam was sampled straight into the detector. A homemade 4096-channel multichannel scaler[34] interfaced with a computer to accumulate the data. The flight path from the wheel to the effective center of the ionizer was experimentally determined to be 30.1 cm. Cl and ozone beam velocity distributions are described by beam parameters such as beam speed (v) and speed ratio ($v/\Delta v$).[35,36] These parameters were determined by the program KELVIN,[35,36] which fitted the beam TOF spectra by making appropriate offset time corrections (ion flight time, wheel trigger time offset, etc.) and convoluting the known apparatus functions. Typical beam parameters are listed in Table 1. Most-probable collision energies E_{coll} and the spread of the collision energies are listed in Table 2.

Product TOF spectra from the reactive scattering were measured by using the cross-correlation method.[37] A 17.8 cm diameter cross-correlation wheel was mounted in front of the detector and was spun at 392 Hz. The wheel has two identical

TABLE 1: Experimental Beam Parameters

beam condition	peak velocity (v_{pk}) (m/s)	speed ratio ($v/\Delta v$)
Cl (1% Cl_2 in He)	3320	5.5
Cl (10% Cl_2 in 82% He and 8% Ar)	2270	5.4
Cl (10% Cl_2 in Ar)	1410	6.7
O_3 (7% in He)	1490	13.6
O_3 (7% in Ar)	640	12.5

TABLE 2: Experimental Conditions

v_{pk} (m/s)				
Cl	O_3	E_{coll} (kcal/mol)	$\Delta E_{coll}/E_{coll}$[a] (%)	$\Delta E_{coll}/E_{avl}$[b] (%)
3320	1490	32	31	14
2270	640	13.5	34	9
1410	640	6	25	3

[a] Collision energy spread (fwhm), relative to collision energy. [b] Collision energy spread (fwhm), relative to total available energy.

255-bit pseudorandom sequences of open and closed slots. When spun at 392 Hz, it gives nominal 5 μs/channel time resolution in the TOF spectra. The mass spectrometer was set at $m/e = 51$ with low resolution to detect more abundant ^{35}ClO isotope species, while a small amount of ^{37}ClO might have been collected as well. Total counting times ranged from 0.5 to 12 h per laboratory angle.

When the detector was within 25° of the ozone beam, the O_3 molecule ($m/e = 48$) elastically scattered by the noble carrier gas in the Cl beam leaked into the ClO ($m/e = 51$) TOF spectra. However, the elastic O_3 TOF peak was well separated from the reactive ClO peak in the flight time, and its intensity was ≤5% of that of the reactive ClO peak. The elastic O_3 peak was scaled and subtracted from the raw ClO TOF spectra at laboratory angles $\Theta \geq 65°$. When measuring ClO TOF spectra near the Cl beam (within 10° of the Cl beam), a small amount of slow effusive background from the Cl beam source showed up in the spectra. The ClO TOF spectra with O_3 beam off were subtracted from those with O_3 beam on at these small laboratory angles ($\Theta \leq 10°$).

ClO product angular distributions were measured by modulating the ozone beam using a 150 Hz tuning folk chopper (Bulova) with the TOF wheel removed. At a particular angle, the signals with the O_3 beam on and off were recorded in two separate channels in a dual-channel scaler (Joerger, Model VS) with an appropriate gating originated from the tuning folk chopper. Subtracting the beam-off signal from the beam-on signal at a particular laboratory angle gave the net reactive signal at that angle. To correct for long-term drifts of the experimental conditions, a reference angle (typically the one with maximum intensity) was chosen. After a sequence of measurements at every 6−10 angles, data were taken twice at this reference angle. The set of data was then normalized by taking a linear interpolation based on the time at which a given angle was measured and the time between normalization measurements. Counting time at each angle in each normalization sequence ranged from 1 to 3 min, while the total counting time per angle summed from all the normalization sequences ranged from 8 to 30 min.

The main scattering chamber was lined with a liquid-nitrogen-cooled cold panel along the walls. To further reduce the background species that may bounce off the surface opposite to the detector and enter into the detector, an additional cryogenically cooled copper panel was placed inside the main chamber against the differential wall and facing the detector. These arrangements were effective in reducing the ClO background for both TOF and angular distribution measurements.

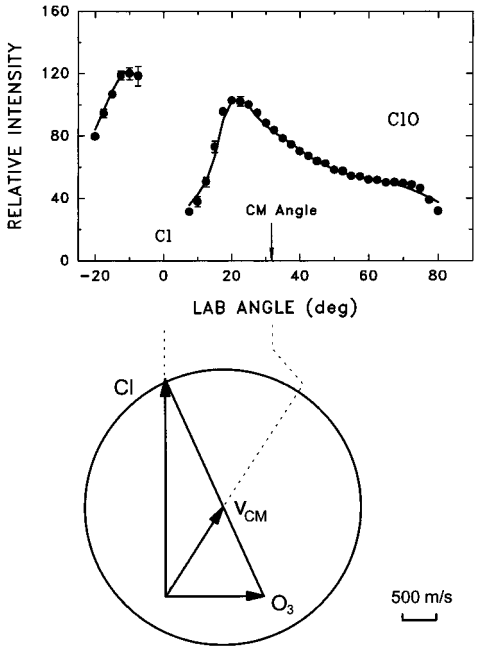

Figure 3. (upper) Laboratory angular distribution of the ClO product in Cl + O_3 reaction at $E_{coll} = 32$ kcal/mol. The filled circles are the experimental data. Error bars stand for 95% confidence limits. The solid lines are for the fitted distribution. (lower) Newton diagram for the reaction Cl + O_3 at $E_{coll} = 32$ kcal/mol. The circle stands for the maximum CM recoil velocity of the ClO product.

III. Results and Analysis

ClO product laboratory angular and TOF distributions were recorded at four CM collision energies from 6 to 32 kcal/mol (Figure 1). Experimental conditions for three collision energies are listed in Table 2. Newton diagrams for these three collision energies are shown in Figures 3, 7, and 11. The circles stand for the maximum range of CM recoil velocity of the ClO product if all the available energy channels into the translational energy of the products. The angular and TOF distributions were recorded at $m/e = 51$, corresponding to $^{35}ClO^+$.

Product laboratory angular distribution and TOF spectra were fitted by a forward-convolution method, using an improved program based on a previous code written by Buss.[38] The goal of the analysis is to find the product angular and translational energy distributions in the CM frame, i.e., the CM flux−energy distribution. In most cases, CM product translational energy and angular distribution $I_{CM}(\theta,E_T)$ (where θ is the CM angle and E_T is the *total* CM product translational energy) is assumed to have a separable form and is expressed as a product of $T(\theta)$, the CM product angular distribution, and $P(E_T)$, the CM product translational energy distribution:

$$I_{CM}(\theta,E_T) = T(\theta)\, P(E_T) \qquad (1)$$

The program transforms this trial CM flux distribution into the laboratory frame flux distribution by using the transformation Jacobian $I_{LAB}(\Theta,v) = I_{CM}(\theta,u)(v^2/u^2)$, where Θ is the laboratory angle and v and u are the laboratory and CM velocity of ClO, respectively. It then generates ClO laboratory angular distribution and TOF spectra for each experimental laboratory angle, after convoluting over the measured beam velocity distributions and the known apparatus functions such as the spread of collision angles, the detector acceptance angles, and the length of the ionizer. The program scales the calculated spectra to the experimental data and makes the comparison. This procedure is repeated so as to optimize the $T(\theta)$ and $P(E_T)$ iteratively until a best fit for the experimental data is found.

Initially, we tried to fit the experimental data by using a single set of separable $T(\theta)$ and $P(E_T)$, as described above. However, it was soon realized that the CM angular distribution $T(\theta)$ and the translational energy distribution $P(E_T)$ were coupled; i.e., the product translational energy release was dependent on the CM scattering angle. In the CM frame, the translational energy release in the forward direction with respect the Cl atom was larger than that in the backward direction. In the laboratory frame, the ClO product was faster at small laboratory angles.

To account for this coupling effect in a simplified way, we used a combination of different sets of separable $T(\theta)$ and $P(E_T)$. The CM product flux distribution was expressed as a weighted sum of the products of different sets of $T(\theta)$ and $P(E_T)$:

$$I_{CM}(\theta,E_T) = \sum_{i=1}^{n} w_i T_i(\theta)\, P_i(E_T) \qquad (2)$$

Each $P_i(E_T)$ was normalized so that $\int P_i(E_T)\, dE_T = 1$. The total CM angular distribution could therefore be expressed as

$$I_{CM}(\theta) = \int_0^\infty I_{CM}(\theta,E_T)\, dE_T = \sum_{i=1}^{n} w_i T_i(\theta) \qquad (3)$$

For our purposes, a trial $I_{CM}(\theta,E_T)$ combined from two different sets of $T(\theta)$ and $P(E_T)$ ($n = 2$ in eq 2) was used as the input to the fitting program. $T(\theta)$ was chosen in a point form, and $P(E_T)$ was chosen to have the following RRK-type functional form:

$$P(E_T) = (E_T - B)^p (E_{avl} - E_T)^q \qquad (4)$$

where E_{avl} is the total available energy and B, p, and q are adjustable fitting parameters. After optimizing this trial $I_{CM}(\theta,E_T)$ function, satisfactory fittings to the experimental data were reached. In principle, using a larger set of functional forms to represent the nonseparable CM flux−energy distribution should give an even better fit.[39−41] In our case, however, two sets of $T(\theta)$ and $P(E_T)$ seem to be able to reproduce the experimental data fairly well. Due to the nature of the coupled $T(\theta)$ and $P(E_T)$, quite a few fitting parameters (mainly in the point forms of the $T(\theta)$) are required to describe the CM flux−energy distribution and to fit the experimental data. Nevertheless, simultaneous fitting of the laboratory angular distribution and near 20 experimental TOF spectra at each collision energy puts tight constraints on these parameters in the forward-convolution procedures, and reliable fits can be obtained. Furthermore, qualitative and global description of the flux−energy distribution (e.g., the flux−energy contour maps) is sufficient to reveal main features of the reaction mechanisms, and the quality of our fittings of the experimental data should provide reliable information to identify these features in the mechanisms. Finally, the fitted flux−energy distribution from the forward convolution can be confirmed by direct conversion of the experimental data. In the direct conversion procedure,[42] no convolution of the beam velocity distributions and apparatus functions is carried out. Only a single Newton diagram (with the most probable or the averaged beam velocities) is used, and the laboratory TOF data are converted to the CM distribution by the transformation Jacobian. Though less accurate, it provides basic features of the CM flux distribution. Our forward convolution results are in agreement with those from the direct conversion.

Experimental and calculated laboratory angular distributions at three collision energies are shown in Figures 3, 7, and 11. Representative experimental and fitted laboratory TOF spectra are shown in Figures 4 and 8 (for E_{coll} = 32 and 13.5 kcal/mol). The total CM angular distributions and relative translational energy distributions $P(E_T)$ at various CM angles are plotted in Figures 5, 9, and 12. Using the optimized CM flux−energy distribution $I_{CM}(\theta,E_T)$, we plot the CM flux distributions in velocity space $I_{CM}(\theta,u)$ [$I_{CM}(\theta,u) \propto uI_{CM}(\theta,E_T)$] in both contour maps and 3-dimensional projections in Figures 6, 10, and 13 for E_{coll} = 32, 13.5, and 6 kcal/mol.

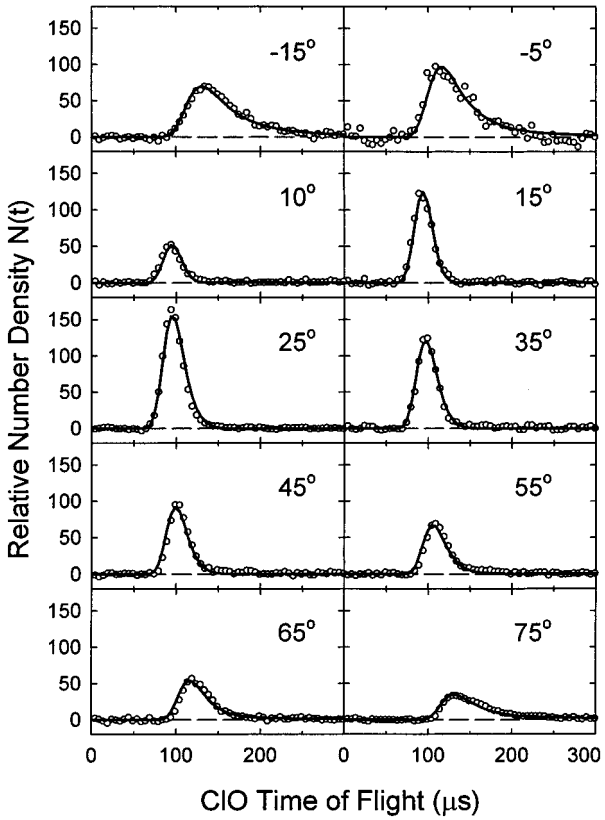

Figure 4. Laboratory TOF spectra of the ClO product at E_{coll} = 32 kcal/mol. The circles are the experimental data points, and the solid lines are the fitted spectra. A total of 19 TOF spectra were taken and fitted at laboratory angles from −20° to 75°, while only 10 are shown here. The spectra are labeled by the laboratory angles.

The measured laboratory angular distributions are quite broad. With collision energy increased, the laboratory angular distribution peaks in the more forward direction. In the CM frame, the angular distributions are also quite broad, and they have predominant intensities in the sideways and forward scattering directions. The CM angular distributions do not have a forward−backward symmetry. As the collision energy increases from 6 to 13.5 and 32 kcal/mol, the peak position of the CM angular distribution shifts from ∼60°−90° to 45° and 30°, and the peak becomes more predominant as well. In the very small CM angle region beyond the peak, the intensities seem to drop rapidly.

CM product translational energy release is large, with its average ranging from ∼35% to ∼65% of the total available energy. All CM translational energy distributions, $P(E_T)$, peak quite far away from 0 kcal/mol; they are smooth and nearly symmetric. The product translational energy release couples with the CM scattering angles; e.g., the product translational energy is greater at small CM angles than at large CM angles (Figures 5, 9, and 12). With the collision energy increased, the product translational energy increases; the translational energy distribution $P(E_T)$ becomes broader; and the angular dependence of the translational energy becomes larger, as shown in Tables 3 and 4 and Figures 5, 9, 12, and 14. However, due to the large reaction exoergicity, product internal energy is also significant, and its fraction in the total energy is larger at low collision energy.

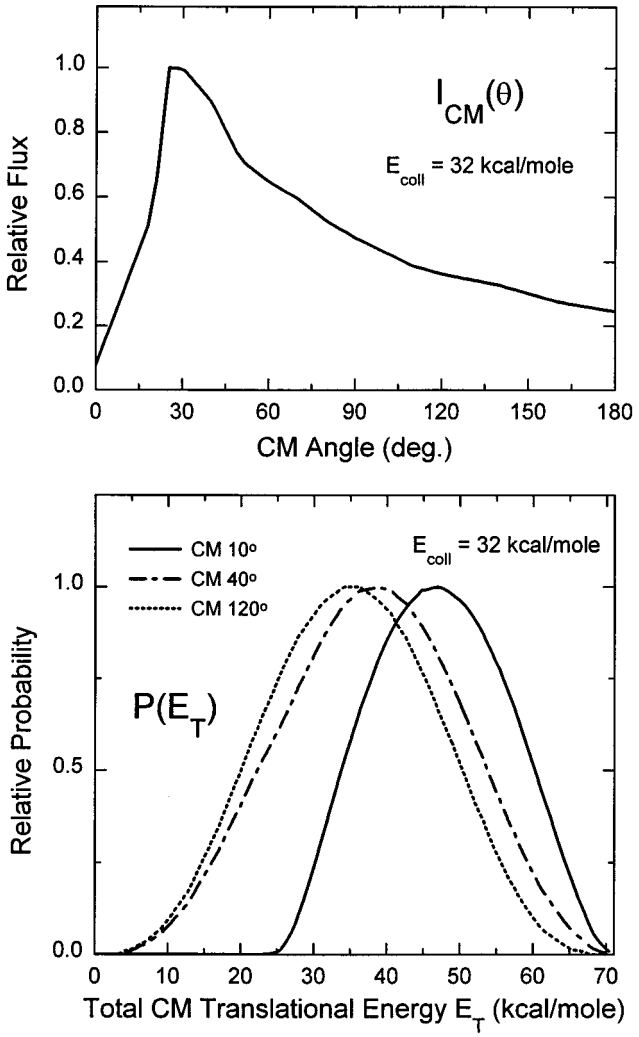

Figure 5. (upper) Total CM angular distribution $I_{CM}(\theta)$ at $E_{coll} = 32$ kcal/mol. The maximum of the relative angular distribution is scaled to unit. (lower) Total CM product translational energy distribution $P(E_T)$ at various CM angles for $E_{coll} = 32$ kcal/mol. Maximum probabilities are scaled to unit. The maximum translational energy is the total available energy at the most probable collision energy $E_{coll} = 32$ kcal/mol.

We also tried to detect the reaction channel $Cl + O_3 \rightarrow ClO_2 + O$ (Figure 1), which is open at ~17.4 kcal/mol collision energy. There are two types of ClO_2 isomers: ClOO and OClO. ClOO is a weakly bound molecule, and the bond energy between Cl and O_2 is only ~5−6 kcal/mol.[43] OClO is a stable molecule and could be observed by the mass spectrometer. However, to make OClO, it might require the insertion of the Cl atom into one of the O−O bonds of the O_3 molecule, and the reaction barrier is expected to be very high. We could not detect any signal at $m/e = 67$ at the high collision energies of 26 and 32 kcal/mol.

IV. Discussion

A. The Reaction Mechanism of $Cl + O_3 \rightarrow ClO + O_2$. The reaction $Cl + O_3 \rightarrow ClO + O_2$ is a direct reaction, since the CM angular distribution does not have the typical forward−backward symmetry that a reaction via a persistent long-lived complex has,[44] and the translational energy release is repulsive and has a strong angular dependence. This conclusion is consistent with ClO_3 energetics derived from the theoretical studies.[21,22] Energy levels of the three ClO_3 isomers all lie above that of the ground-state products according to *ab initio* calculations (Figure 1);[21,22] the asymmetric ClO_3 is even unstable on higher levels of calculations.[22] The asymmetric ClO_3 could not be a persistent long-lived complex due to the absence of a potential well and due to the large excess energy in the exit channel. Observations by Carter and Andrews in matrix spectroscopy work also confirmed that an asymmetric long-lived complex was not likely involved in the $Cl + O_3$ reaction.[14]

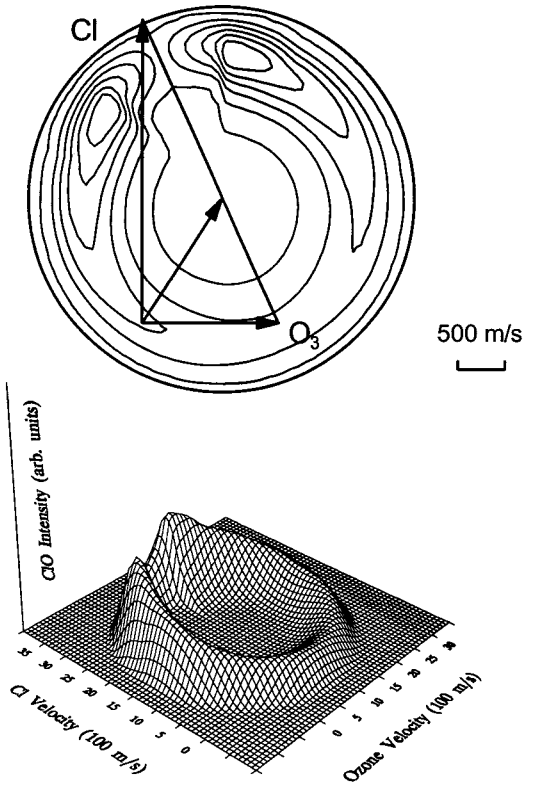

Figure 6. Contour map and 3-D plot for the CM ClO flux−velocity distribution $I_{CM}(\theta,u)$ at $E_{coll} = 32$ kcal/mol.

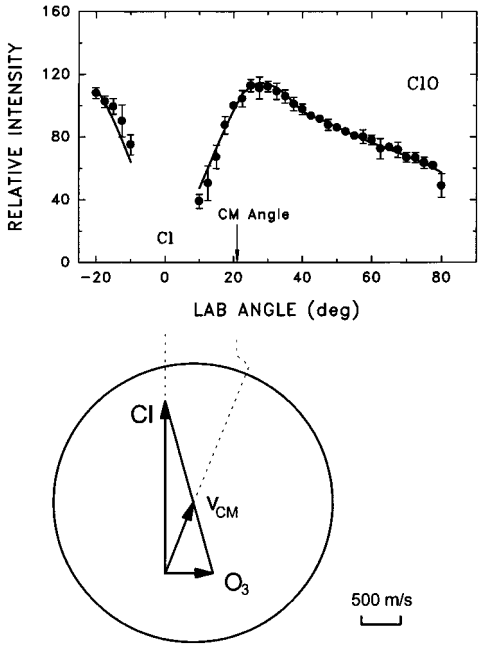

Figure 7. Same as Figure 3 but at $E_{coll} = 13.5$ kcal/mol.

Electronic structure of ozone plays an important role in the reaction mechanism.[23] The ground electronic state of the O_3 molecule is 1^1A_1 in C_{2v} symmetry, and its electronic configuration is[45−48] $...(5a_1)^2(3b_2)^2(1b_1)^2(6a_1)^2(4b_2)^2(1a_2)^2(2b_1)^0$. Two terminal atomic O $2p\pi$ orbitals form the pair of the π molecular orbitals $1a_2$ and $2b_1$. The highest occupied molecular orbital (HOMO) is $1a_2$, fully occupied by two terminal O $2p\pi$ electrons, while the lowest unoccupied molecular orbital (LUMO) is $2b_1$.

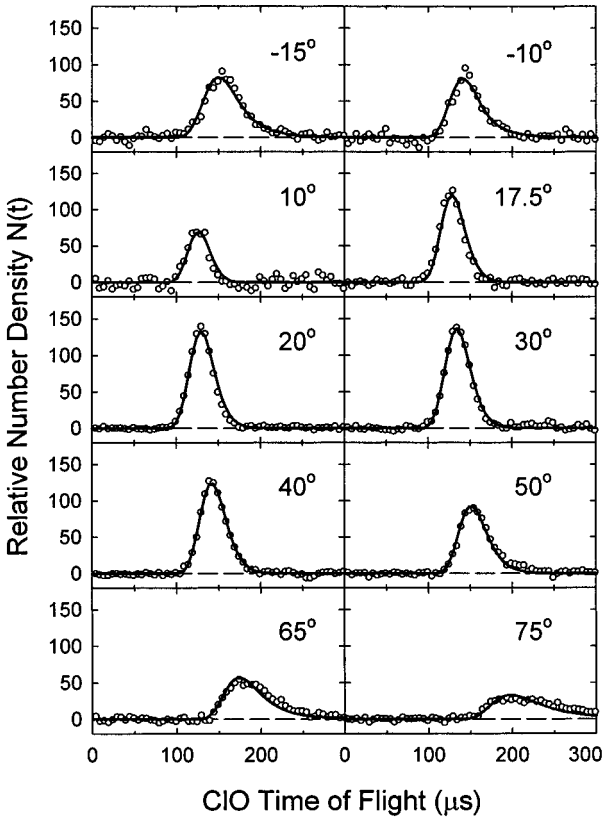

Figure 8. Same as Figure 4 but at E_{coll} = 13.5 kcal/mol. Ten of the 18 TOF spectra are shown here.

Ozone can also be characterized as a diradical with two unpaired π electrons on the two terminal oxygen atoms.[45] The central oxygen atom has a closed outer shell of eight electrons, and a terminal oxygen atom has only seven outer electrons with a half-filled 2pπ orbital perpendicular to the molecular plane.

The electronic structure of the ozone molecule suggests that it is unlikely for the Cl atom to abstract the central oxygen atom, because of the large repulsion of the lone-pair electrons on the central oxygen atom. Furthermore, if the Cl atom abstracted the central oxygen atom in a coplanar approach, the ClO product would be predominantly scattered to the backward direction in a direct reaction mechanism, and the O_2 molecule formed from the terminal O atoms should be highly vibrationally excited. However, our experimental results show that the ClO CM angular distribution peaks predominantly sideways and forward instead of backward, indicating that the Cl atom is unlikely to abstract the central O atom.

It is also unlikely for the Cl atom to insert into the O−O bond. Previous kinetic studies of this reaction suggested that the transition-state structure closely resembled that of the stable ozone molecule.[7−12] We have also studied the reaction Br + O_3 by using the crossed molecular beams technique,[49] and the results for both the Cl + O_3 and the Br + O_3 reactions are very similar, suggesting that the transition-state configurations of these two reactions are similar and the Cl or Br atom probably does not insert into the O−O bond to make a quite different transition-state structure from that of the stable ozone molecule. The insertion of the Cl atom into the O−O bond is also not favored according to the frontier orbital theory.[50] In this pathway, there is no effective orbital overlap and interaction. Unless the collision energy is very high, this pathway is not expected to be significant.

The Cl atom is most likely to abstract the terminal oxygen atom. One way is that it approaches a terminal π orbital perpendicularly to the ozone molecule plane, which is the similar reaction pathway given in the *ab initio* calculations of the H + O_3 reaction.[23] This is the favorite way in the frontier orbital theory,[50] as the HOMO of ozone could be considered as two

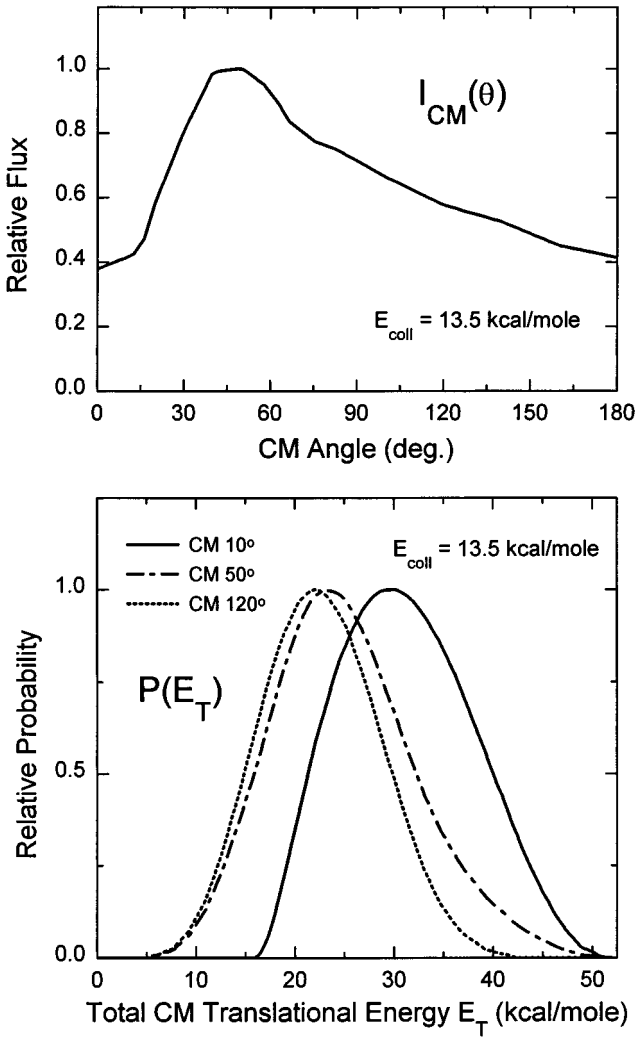

Figure 9. Same as Figure 5 but at E_{coll} = 13.5 kcal/mol.

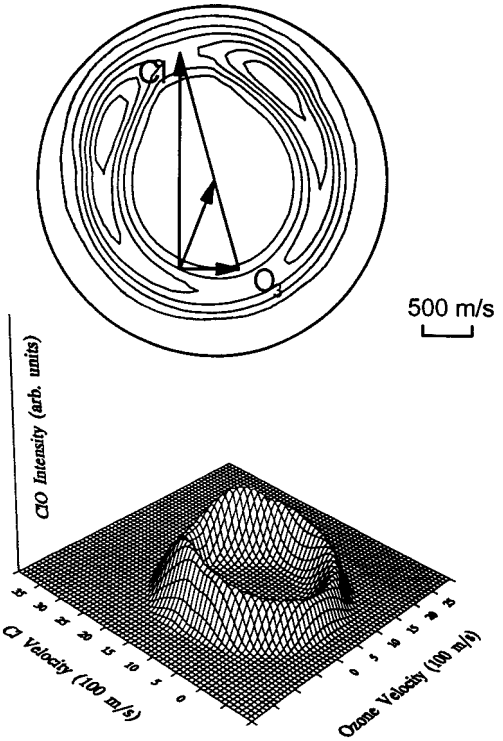

Figure 10. Same as Figure 6 but at E_{coll} = 13.5 kcal/mol.

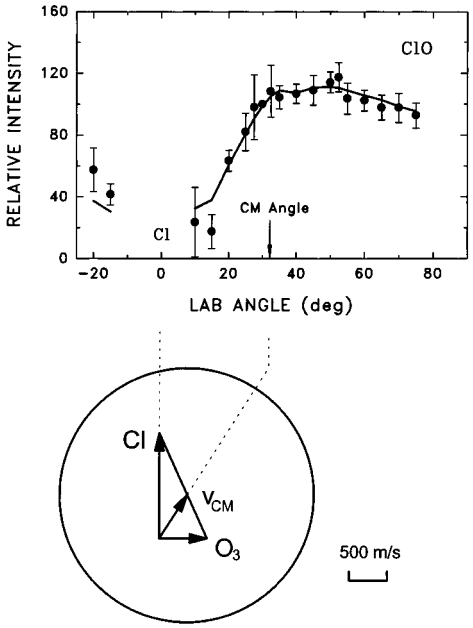

Figure 11. Same as Figure 3 but at $E_{coll} = 6$ kcal/mol.

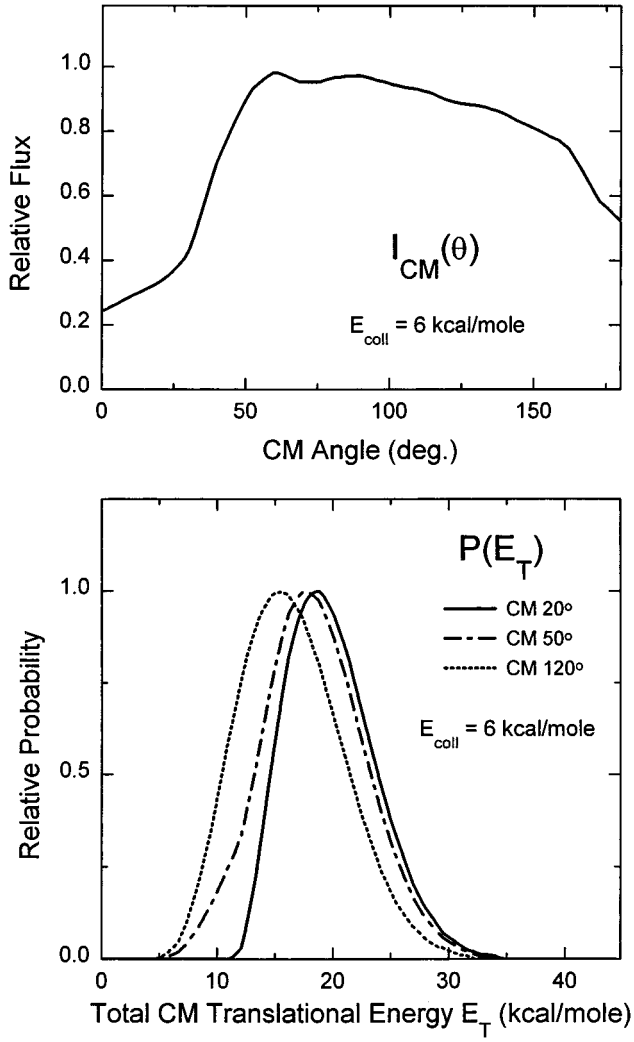

Figure 12. Same as Figure 5 but at $E_{coll} = 6$ kcal/mol.

weakly coupled 2pπ orbitals on the two terminal O atoms. When the singly occupied p orbital of the Cl atom descends vertically to the π orbital on a terminal O atom, the interaction between these two orbitals has a net overlap and is symmetry-allowed. This collision pathway has a large impact parameter since the center of mass of ozone is on the C_{2v} axis that goes through the central O atom, and the ClO product tends to be scattered in the forward direction. As the collision energy increased, the forward scattering becomes more predominant. However, this large impact parameter pathway could not explain the significant amount of wide-angle scattering observed, especially at high collision energies.

A coplanar reaction mechanism, in which the Cl atom attacks a terminal O atom in the ozone molecule plane, could explain the experimental results, especially for the sideways and wide-angle scattering. A bent transition state in the coplanar collision pathway is expected from the bent ozone molecule, in consistency with the observed sideways scattering. In the coplanar reaction pathway, the Cl atom can have a large range of attacking angles, and for a direct reaction, such a large range of attacking angles correspond to a wide range of CM angles into which the ClO product is scattered. For example, if the Cl atom approaches the ozone molecule along the direction of

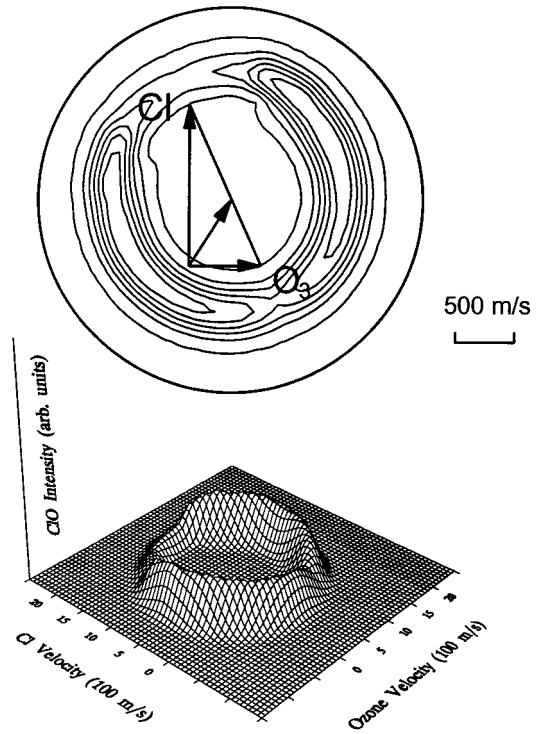

Figure 13. Same as Figure 6 but at $E_{coll} = 6$ kcal/mol.

TABLE 3: Average Translational Energy Release

		$\langle E_T\rangle/E_{avl}$[c]			
E_{coll}[a]	E_{avl}[b]	CM angle 10°	CM angle 50°	CM angle 120°	$(\Delta\langle E_T\rangle)_{max}$[d]
32	71	0.66	0.50	0.49	12.2
13.5	52.5	0.60	0.47	0.43	8.6
6	45	0.43	0.41	0.37	2.7

[a] Collision energy in kcal/mol. [b] Total available energy in kcal/mol. [c] Fraction of average product translational energy at various CM angles. [d] Maximum difference of average translational energy release at small and large CM angles in kcal/mol.

TABLE 4: Peak Translational Energy Release

		E_T^{peak}/E_{avl}[a]			
E_{coll}	E_{avl}	CM angle 10°	CM angle 50°	CM angle 120°	$(\Delta E_T^{peak})_{max}$[b]
32	71	0.65	0.55	0.49	11.0
13.5	52.5	0.56	0.44	0.42	7.2
6	45	0.41	0.40	0.35	2.8

[a] Fraction of peak product translational energy at various CM angles. [b] Maximum difference of peak translational energy release at small and large CM angles in kcal/mol.

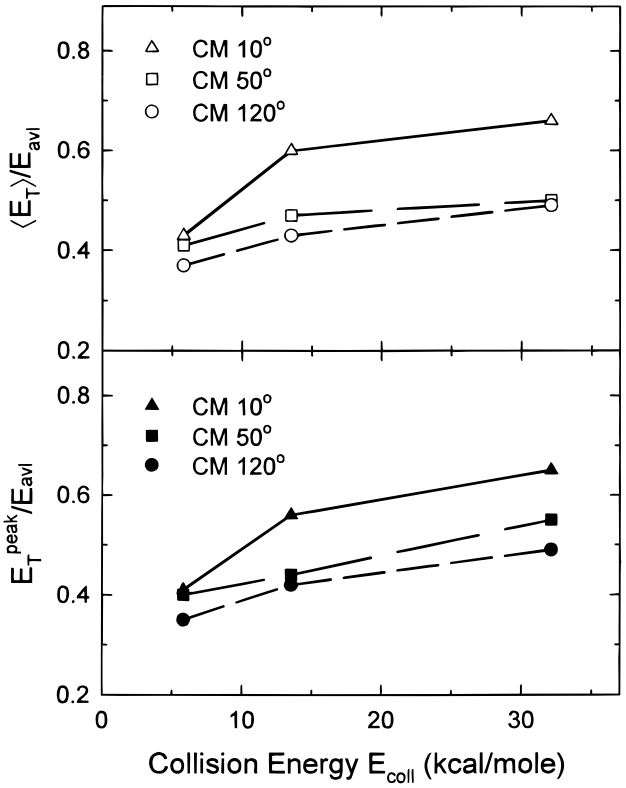

Figure 14. (upper) Fraction of average translational energy in the total available energy at different CM angles versus collision energies. (lower) Fraction of peak translational energy at different CM angles versus collision energies.

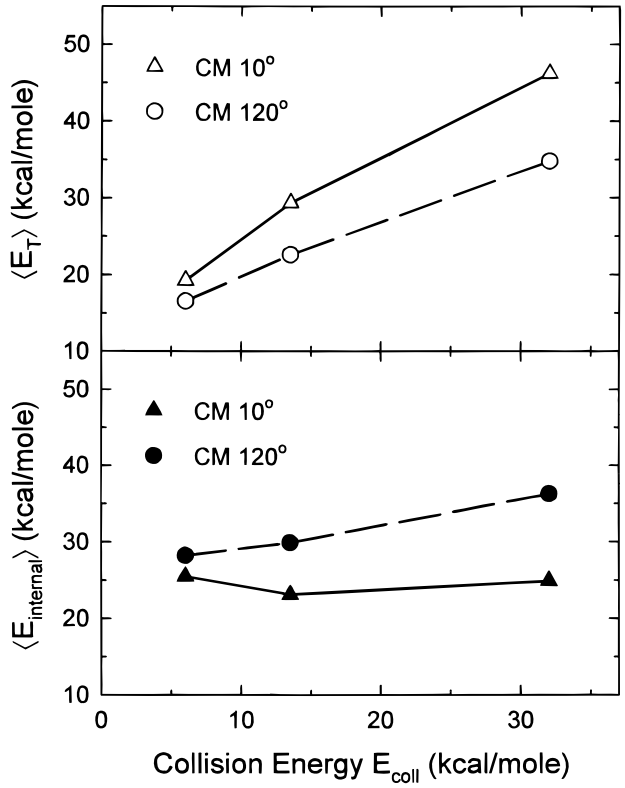

Figure 15. (upper) Average translational energy at different CM angles versus collision energies. (lower) Average internal energy at different CM angles versus collision energies.

the terminal and central O atoms, some backward scattered ClO would be expected. However, if the Cl atom attacks perpendicularly to the axis of the terminal and central O atoms, the ClO product could be sideways and forward scattered.

It is possible that the Cl + O_3 reaction proceeds through two reaction mechanisms: a coplanar and an out-of-plane reaction pathway. Note that, while the product translational energy increases with the collision energy at all CM angles, the rate of increase differs with CM angles (Figures 14 and 15). Specifically, the product translational energy increases faster for small CM angles (e.g., for $\theta = 10°$, $d\langle E_T \rangle / dE_{coll} \approx 1$) than for large CM angles (e.g., for $\theta = 120°$, $d\langle E_T \rangle / dE_{coll} \approx 0.7$); the internal energy remains nearly constant for small scattering angels ($\theta = 10°$) (Figure 15). There seems to be a jump in the translational energy release from $E_{coll} = 6$ kcal/mol to $E_{coll} = 13.5$ kcal/mol at CM angle 10°, while there is only smooth increase at CM angle 120° (Figure 14). Similar behaviors have been observed in the Br + O_3 reaction.[49] These two different types of collision energy dependences might suggest two reaction pathways. It appears that at $E_{coll} = 6$ kcal/mol the forward scattering with larger translational energy release is a minor channel, and it may have a higher effective reaction barrier than the wide-angle scattering channel. In a large impact-parameter collision such as the out-of-plane approach, a significant fraction of the translational energy is tied up as the rotational energy of reaction intermediate (centrifugal energy), and it will not be effective in overcoming the potential energy barrier of the entrance channel, especially when the translational energy is low. Only at higher collision energies, the large impact-parameter collision in the out-of-plane approach becomes significant; the large translational energy release is consistent with the significant centrifugal energy and the forward scattering. Of course, the analysis for the out-of-plane collision is also applicable for the large impact-parameter collision in the in-plane approach. However, in the coplanar approach, the impact parameter and attacking angle dependence of the product scattering angle and energy release should be smooth; therefore, the considerable change in CM angle dependence of the translational energy release may not solely come from the in-plane pathway.

A repulsive energy release is quite evident from the translational energy distribution, which peaks far away from 0 (Figures 5, 9, and 12). Furthermore, extrapolation of the product translational energy release reveals that it is ~33% of the reaction exoergicity near the reaction threshold (Figure 15), in consistency with an impulsive energy release model which predicts that 40% of the exoergicity goes into the translation at the threshold.[41] The repulsive energy release is also manifested by the CM angular distribution and its collision energy dependence. At low collision energy ($E_{coll} = 6$ kcal/mol), the repulsion from O−O bond rupture is strong compared with the initial forward impulse from the Cl atom; the ClO product is mainly sideways scattered. As the collision energy increased, the forward impulse from the Cl atom in the large impact parameter collision starts to overcome the sideways repulsion; the forward peak becomes more predominant. However, the intensity falls off within CM angle 20°, indicating that the repulsive energy release is still significant even compared with the highest collision energy.

At low collision energy ($E_{coll} = 6$ kcal/mol), the ClO product is mainly sideways scattered, and the average or peak translational energy is about 40% of the total energy. The coplanar collision channel seems to contribute dominantly at $E_{coll} = 6$ kcal/mol. Assuming that at thermal collision energy (~1 kcal/mol) the product translational energy release is ~35% of the total available energy, and using the fact that the peak nascent ClO vibrational population is $v \approx 8$ (peak E_{vib}(ClO) is ~19 kcal/mol, or 47% of the total available energy), the maximum value of the peak vibrational energy of O_2 is ~7 kcal/mol, corresponding to a peak vibrational level up to 1, and this value is smaller when taking the rotational energy of ClO into account.

Therefore, O_2 should have a very small amount of internal energy. At high collision energies (E_{coll} = 13.5 and 32 kcal/mol), the ClO product is forward and sideways scattered, and the translational energy is about 40−65% of the total energy. In summary, the in-plane pathway is essential for the sideways and wide-angle scattering, and it also contributes to the forward scattering. This in-plane pathway is the major, if not exclusive, channel at all collision energies, especially at low collision energy. A possible out-of-plane collision pathway could contribute to the forward scattering as well, and this pathway seems to become important at high collision energy. Also, the forward scattering channel is very efficient in channeling the collision energy into the products' translation.

Our experimental results agree qualitatively with Farantos and Murrell's semiempirical calculations.[20] The Cl + O_3 reaction is a direct reaction, and no long-lived complex is involved. Product translational energy is about 50% of the total available energy. Our conclusion that the Cl atom could attack the ozone molecule in a coplanar way is consistent with the collinear reaction pathway on the semiempirical ClO_3 PES. Similarity of our experimental results for both the Cl + O_3 reaction and the Br + O_3 reaction[49] is consistent with an early transition state that resembles the reactant ozone molecule, as suggested by the semiempirical studies[20] and previous kinetic studies.[9,10] Although the translational energy release is large, product internal energy is also significant due to the large reaction exoergicity. The internal energy of the products, though not resolved in this experiment, is expected to be mainly the vibrational and rotational energy of the ClO product for a reaction via early transition state. Indeed, this has been shown in the semiempirical calculations[20] and is consistent with the measured ClO vibrational-state distributions.[15−17]

Quantitative comparison between the experiment and the calculation, however, is not satisfactory. For example, couplings of translational energy release and CM scattering angles were not demonstrated in the calculations. The most noteworthy discrepancies are in the CM angular distributions. The calculations showed that ClO product peaked sharply in the forward direction at a thermal collision energy of ∼1 kcal/mol, while the experimental CM angular distribution at 6 kcal/mol collision energy, the lowest in our experiment, is relatively flat and peaks sideways. Only with the collision energy increased to 13.5 and 32 kcal/mol does the CM angular distribution shift to the forward direction. Strictly speaking, the CM angular distribution at higher collision energy is not totally forward but forward-sideways peaked. The intensity at $\theta < 20°$ in the CM angular distribution is still small even at the highest collision energy. One possible reason for these discrepancies is that the semiempirical PES does not have a strong enough repulsion on the exit channel. It has been suggested that electron density is transferred from the HOMO of ozone to the singly occupied p orbital on the Cl atom, as the Cl atom has higher electron affinity but lower ionization potential than the O_3 molecule.[9,10] The O−O bond could be substantially weakened, and a strong repulsion between the remaining O_2 and the newly formed ClO can channel a large amount of energy into the products' translation. Our experimental results also suggest a possible out-of-plane collision pathway, but the semiempirical studies failed to explore this possible approach.[20] The out-of-plane pathway was favored by the *ab initio* calculations of the H + O_3 reaction,[23] as the H atom has only an s orbital and prefers to have a σ-type interaction in the out-of-plane approach rather than a repulsive interaction in the in-plane approach. However, the key features of the H + O_3 PES may not be totally transferable to the Cl + O_3 reaction, since our experimental results show that the in-plane collision channel in the Cl + O_3 reaction has a major contribution. This may be due to the fact that the Cl p orbital can have a $\pi-\pi$ interaction with the terminal O atom in a coplanar approach. Over all, an *ab initio* calculation on the Cl + O_3 reaction is very desirable for comparing with the crossed molecular beam study.

B. The Absence of Electronically Exited O_2 Products. Three ClO + O_2 channels are spin-allowed and energetically possible (Figure 1). In a coplanar collision pathway, the reaction proceeds through a C_s symmetry. Three product channels can correlate with the reactants via $^2A'$ or $^2A''$ states. However, no evidence for the electronically excited $O_2(^1\Delta_g)$ and $O_2(^1\Sigma_g^+)$ channels was found.[18,19] In our experiment, the translational energy distributions are very smooth and extend near the maximum available energy, suggesting a primary ground-state $O_2(^3\Sigma_g^-)$ channel as well. This is also consistent with the fact that a large fraction of the internal energy is in ClO vibration.[17] Dominant production of ground-state O_2 seems to be a general case in the radical and ozone reactions such as Cl + O_3,[18,19] $O(^3P)$ + O_3,[51] $H(^2S)$ + O_3,[51] and $NO(^2\Pi)$ + O_3.[51,52] This phenomenon might be understood via the ozone electronic structure. When the radical attacks a terminal oxygen atom and the O−O bond between this terminal oxygen atom and the central oxygen atom cleaves, the remaining O−O part of the ozone molecule can readily form the ground-state $O_2(^3\Sigma_g^-)$, as the old π orbitals on this O−O section have already had the correct configuration of the triplet ground state and change of electronic energy and structure is minimum. However, to form the excited singlet $O_2(^1\Delta_g)$ molecule, the unpaired electron on the central oxygen atom that has just been released from the breaking of the O−O σ bond has to undergo unfavorable rearrangement to pair with the previously unpaired π electron on the terminal oxygen atom. If the radical attacks the central oxygen atom instead of the terminal oxygen atom, a large change of the O−O electronic structure could occur, and the electronically excited O_2 might form;[53] however, this approach will encounter a very high barrier, and our experimental results imply that the Cl atom would not likely attack the central oxygen atom. Following the above analysis, it is not surprising that almost no electronically excited O_2 molecule is produced in the Cl + O_3 reaction.

C. The Absence of the ClOO and OClO Channels. The reaction channels Cl + O_3 → $ClOO(^2A)$ + $O(^3P)$ ($\Delta H° \approx 17.4$ kcal/mol) and Cl + O_3 → $OClO(^2A)$ + $O(^3P)$ ($\Delta H° \approx 19.5$ kcal/mol) are energetically open at the high collision energies of 26 and 32 kcal/mol, and they are spin-allowed. However, we have not observed any evidence of these two channels. To produce OClO, the Cl atom has to insert into the ozone molecule, but the high repulsion barrier will prohibit this reaction channel. When the Cl atom attacks a terminal oxygen atom to form the asymmetric ClO_3 intermediate, it would be the O−O bond between this terminal oxygen atom and the central oxygen atom that is weakened the most and breaks. It is unlikely for the other O−O bond to break to form the weakly bound ClOO product.

D. Spin−Orbit States of the Reactant Cl Atom and the Product ClO Radical. Cl atoms are generated in two spin−orbit states $Cl(^2P_{3/2})$ and $Cl(^2P_{1/2})$. The excited state $Cl(^2P_{1/2})$ is separated by 2.52 kcal/mol from the ground state $Cl(^2P_{3/2})$. Assuming a Boltzmann distribution, about 20% of the Cl atoms are in the spin−orbit excited state $Cl(^2P_{1/2})$ at 1800 K temperature of the thermal dissociation source. However, after the supersonic expansion, $Cl(^2P_{1/2})$ atoms could be partially relaxed. Note that the translational temperature of the Cl atom beam is estimated to be less than 200 K by using the measured speed ratios.[54] For the ClO product, there are two spin−orbit levels in the ground electronic state: $ClO(^2\Pi_{3/2})$ and $ClO(^2\Pi_{1/2})$, which

are separated by 0.91 kcal/mol. The translational energy resolution and the spread of collision energies in our experiment prevented us from getting any information about the reactivities of the two Cl spin−orbit states and the fine-structure populations of the ClO product. In general, the Cl($^2P_{3/2}$) atom is found to be more reactive than the excited Cl($^2P_{1/2}$) atom, except near the reaction threshold,[55] and it has been shown that at 298 K the rate constant of Cl($^2P_{3/2}$) + O_3 is slightly larger than that of Cl($^2P_{1/2}$) + O_3.[7]

V. Conclusions

We have studied the Cl + O_3 reaction by using the crossed molecular beams technique. CM product angular and translational energy distributions have been derived from experimental results. The average translational energy of the products is found to be 35−65% of the total available energy. In the CM frame, the ClO product is sideways and forward scattered with respect to the Cl atom. As the collision energy increased, the ClO product is scattered in a more forward direction. Product translational energy distribution couples with the CM scattering angle. The translational energy release in the forward scattering is larger than that in the wide angle scattering.

The Cl + O_3 reaction is a direct reaction. The Cl atom would most likely abstract a terminal oxygen atom on the ozone molecule. An asymmetric covalently bound ClO_3 complex is unlikely to exist. An early transition state is suggested. The exit channel on the ClO_3 PES is believed to have a strong repulsion. Besides the large product translational energy release, ClO vibration should also be highly excited. A detailed measurement of the internal-state distributions of the ClO and O_2 products would be helpful to complete the picture of the reaction mechanism. An *ab initio* calculation on the Cl + O_3 reaction is desirable to compare with the results of this crossed molecular beam study.

Acknowledgment. We thank T. T. Miau for his assistance. This work was supported by the Director, Office of Energy Research, Office of Basic Energy Sciences, Chemical Sciences Division of the U.S. Department of Energy, under Contract DE-AC03-76SF00098.

References and Notes

(1) Wayne, R. P. *Chemistry of Atmospheres*; Clarendon Press: Oxford, 1991.
(2) Molina, L. T.; Molina, M. J. *J. Phys. Chem.* **1987**, *91*, 433.
(3) McElroy, M. B.; Salawitch, R. J.; Wofsy, S. C.; Logan, J. A. *Nature* **1986**, *321*, 759.
(4) Anderson, J. G.; Toohey, D. W.; Brune, W. H. *Science* **1991**, *251*, 39.
(5) Barrett, J. W.; Solomon, P. M.; de Zafra, R. L.; Jaramillo, M.; Emmons, L.; Parrish, A. *Nature* **1988**, *336*, 455.
(6) Solomon, S. *Nature* **1990**, *347*, 347.
(7) Clyne, M. A. A.; Nip, W. S. *J. Chem. Soc., Faraday Trans. 2* **1976**, *72*, 838.
(8) Zahniser, M. S.; Kaufman, F.; Anderson, J. G. *Chem. Phys. Lett.* **1976**, *37*, 226.
(9) Toohey, D. W.; Brune, W. H.; Anderson, J. G. *Int. J. Chem. Kinet.* **1988**, *20*, 131 and references therein.
(10) Nicovich, J. M.; Kreutter, K. D.; Wine, P. H. *Int. J. Chem. Kinet.* **1990**, *22*, 399 and references therein.
(11) Patrick, R.; Golden, D. M. *J. Phys. Chem.* **1984**, *88*, 491.
(12) (a) Baulch, D. L.; Cox, R. A.; Hampson, R. F. Jr; Kerr, J. A.; Troe, J.; Watson, R. T. *J. Phys. Chem. Ref. Data* **1980**, *9*, 295. (b) Baulch, D. L.; Cox, R. A.; Crutzen, P. J.; Hampson, R. F. Jr.; Kerr, J. A.; Troe, J.; Watson, R. T. *J. Phys. Chem. Ref. Data*. **1982**, *11*, 327.
(13) (a) Prasad, S. S.; Adams, W. M. *J. Photochem.* **1980**, *13*, 243. (b) Prasad, S. S. *Nature* **1980**, *285*, 152.
(14) Carter, R. O. III; Andrews, L. *J. Phys. Chem.* **1981**, *85*, 2351.
(15) (a) McGrath, W. P.; Norrish, R. G. W. *Z. Phys. Chem. (Munich)* **1958**, *15*, 245. (b) McGrath,W. P.; Norrish, R. G. W. *Proc. Roy. Soc. London, A* **1960**, *254*, 317.
(16) Baumgärtel, S.; Gericke, K.-H. *Chem. Phys. Lett.* **1994**, *227*, 461.
(17) Matsumi, Y.; Nomura, S.; Kawasaki, M.; Imamura, T. *J. Phys. Chem.* **1996**, *100*, 176.
(18) Vanderzanden, J. W.; Birks, J. W. *Chem. Phys. Lett.* **198**, *88*, 109.
(19) Choo, K. Y.; Leu, M. *J. Phys. Chem.* **1985**, *89*, 4832.
(20) Farantos, S. C.; Murrell, J. N. *Int. J. Quantum Chem.* **1978**, *14*, 659.
(21) (a) Rathmann, T.; Schindler, R. N. *Chem. Phys. Lett.* **1992**, *190*, 539. (b) Rathmann, T.; Schindler, R. N. *Ber. Bunsen-Ges. Phys. Chem.* **1992**, *96*, 421.
(22) Rauk, A.; Tschuikow-Roux, E.; Chen, Y.; McGrath, M. P.; Radom, L. *J. Phys. Chem.* **1993**, *97*, 7947.
(23) (a) Chen, M. M. L.; Wetmore, R. W.; Schaefer, H. F. III *J. Chem. Phys.* **1981**, *74*, 2938. (b) Dupuis, M.; Fitzgerald, G.; Hammond, B.; Lester, W. A.; Schaefer, H. F., III *J. Chem. Phys.* **1986**, *84*, 2691.
(24) (a) Anlauf, K. G.; MacDonald, R. G.; Polanyi, J. C. *Chem. Phys. Lett.* **1968**, *1*, 619. (b) Polanyi, J. C.; Sloan, J. J. *Int. J. Chem. Kinet. Symp.* **1975**, *1*, 51.
(25) (a) Lee, Y. T.; McDonald, J. D.; LeBreton, P. R.; Herschbach, D. R. *Rev. Sci. Instrum.* **1969**, *40*, 1402. (b) Sparks, R. K. Ph.D. Thesis, University of California, Berkeley, 1979.
(26) Brink, G. O. *Rev. Sci. Instrum.* **1966**, *37*, 857, 1626.
(27) (a) Daly, N. R. *Rev. Sci. Instrum.* **1960**, *31*, 264. (b) Gibbs, H. M.; Commins, E. D. *Rev. Sci. Instrum.* **1966**, *37*, 1385.
(28) Valentini, J. J.; Coggiola, M. J.; Lee, Y. T. *Rev. Sci. Instrum.* **1977**, *48*, 58.
(29) Cook, G. A.; Kiffer, A. D.; Klumpp, C. V.; Malik, A. H.; Spence, L. A. *Adv. Chem. Ser.* **1959**, *21*, 44.
(30) Clough, P. N.; Thrush, B. A. *Chem. Ind.* **1966**, *19*, 1971.
(31) Atyaksheva, L. F.; Emel'yanova, G. I. *Russ. J. Phys. Chem.* **1990**, *64*, 1741.
(32) Griggs, M. *J. Chem. Phys.* **1968**, *49*, 857.
(33) Molina, L. T.; Molina, M. J. *J. Geophys. Res.* **1986**, *91* (D13), 14501.
(34) Weiss, P. S. Thesis, P.h D. California, Berkeley, 1986.
(35) Vernon, M. F. Thesis, P.h D. California, Berkeley, 1983.
(36) Krajnovich, D. J. Thesis, P.h D. California, Berkeley, 1983.
(37) (a) Sköld, a K. *Nucl. Instrum. Methods* **1968**, *63*, 114. (b) Hirshy, V. L.; Aldridge, J. P. *Rev. Sci. Instrum.* **1971**, *42*, 381. (c) Comsa, G.; David, R.; Schumacher, B. J. *Rev. Sci. Instrum.* **1981**, *52*, 789.
(38) Buss, R. J. Thesis, P.h D. California, Berkeley, 1979.
(39) Gillen, K. T.; Rulis, A. M.; Bernstein, R. B. *J. Chem. Phys.* **1971**, *54*, 2831.
(40) Siska, P. E. *J. Chem. Phys.* **1973**, *59*, 6052.
(41) Riley, S. J.; Siska, P. E.; Herschbach, D. R. *Discuss. Faraday Soc.* **1979**, *67*, 27.
(42) (a) Tully, F. P.; Cheung, N. H.; Haberland, H.; Lee, Y. T. *J. Chem. Phys.* **1980**, *73*, 4460. (b) Sparks, R. K.; Shobatake, K.; Carlson, L. R.; Lee, Y. T. *J. Chem. Phys.* **1981**, *75*, 3838.
(43) (a) Nicovich, J. M.; Kreutter, K. D.; Schackelford, C. J.; Wine, P. H. *Chem. Phys. Lett.* **1991**, *179*, 367. (b) Mauldin, R. L., III; Burkholder, J. B.; Ravishankara, A. R. *J. Phys. Chem.* **1992**, *96*, 2582.
(44) (a) Miller, W. B.; Safron, S. A.; Herschbach, D. R. *Discuss. Faraday Soc.* **1967**, *44*, 108. (b) W. B. Miller, Ph.D. Thesis, Harvard University, 1969.
(45) Hay, P. J.; Dunning, T. H., Jr. *J. Chem. Phys.* **1977**, *67*, 2290.
(46) Rothenberg, S.; Schaefer, H. F., III *Mol. Phys.* **1970**, *21*, 317.
(47) Messmer, R. P.; Salahub, D. R. *J. Chem. Phys.* **1976**, *65*, 779.
(48) Borowski, P.; Andersson, K.; Malmqvist, P.-A.; Roos, B. O. *J. Chem. Phys.* **1992**, *97*, 5568.
(49) Zhang, J.; Miau, T. T.; Lee, Y. T. *J. Phys. Chem.*, in press.
(50) (a) Fukui, K. *Reactivity and Structure Concepts in Organic Chemistry*; Springer-Verlag: New York, 1975; Vol. 2. (b) Fukui, K. In *Molecular Orbitals in Chemistry, Physics and Biology*; Löwdin, P.-O., Pullman, B.; Eds.; Academic: New York, 1964; p 513.
(51) Washida, N.; Akimoto, H.; Okuda, M. *Bull. Chem. Soc. Jpn.* **1980**, *53*, 3496.
(52) Gauthier, M.; Snelling, D. R. *Chem. Phys. Lett.* **1973**, *20*, 178.
(53) Redpath, A. E.; Menzinger, M.; Carrington, T. *Chem. Phys.* **1978**, *27*, 409.
(54) Miller, D. R. In, *Atomic and Molecular Beam Methods*; Scoles, G., Ed.; Oxford University Press: Oxford, 1988; Vol. I.
(55) Dagdigian, P. J.; Campbell, M. L. *Chem. Rev.* **1987**, *87*, 1.